ADVANCED ELECTRONIC MATERIALS
www.advelectronicmat.de

Universal Scaling Law for the Size Effect on Superelasticity at the Nanoscale Promotes the Use of Shape-Memory Alloys in Stretchable Devices

*Valeria Fuster, José F. Gómez-Cortés, María L. Nó, and Jose M. San Juan**

Shape-memory alloys (SMAs) are the most stretchable metallic materials thanks to their superelastic behavior associated with the stress-induced martensitic transformation. This property makes SMAs of potential interest for flexible and wearable electronic technologies, provided that their properties will be retained at small scale. Nanocompression experiments on Cu-Al-Be SMA single crystals demonstrate that micro- and nanopillars, between 2 µm and 260 nm in diameter, exhibit a reproducible superelastic behavior fully recoverable up to 8% strain, even at the nanoscale. Additionally, these micro-/nanopillars exhibit a size effect on the critical stress for superelasticity, which dramatically increases for pillars smaller than ≈1 µm in diameter, scaling with a power law of exponent $n = -2$. The observed size effect agrees with a theoretical model of homogeneous nucleation of martensite at small scale and the universality of this scaling power law for Cu-based SMAs is proposed. These results open new directions for using SMAs as stretchable conductors and actuating devices in flexible and wearable technologies.

1. Introduction

Flexible electronic and wearable technologies have emerged at the beginning of the XXI century and in the present decade an extremely high effort is being devoted to develop highly stretchable materials for wearable electronics,[1,2] including a diversity of materials such as flexible semiconductors,[3] or flexible meta-materials,[4] for instance, giving place to a plethora of unforeseen applications.[5] New advances in small-scale soft robots,[6] and particularly in stretchable electronic skin,[7] are driving new fields like functional neural interfaces,[8] and implantable bioelectronics.[9] With a growing worldwide forecast market, which will exceed 200 billion dollars per year by 2027,[10] flexible and stretchable electronic and wearable technologies constitute a new paradigm in the materials science era. Most of these technologies rely on organic materials,[2,11] including shape memory polymers.[12] Nevertheless, in a recent road map in this field,[8] the key points for electrical connectors or electrode materials were well identified: exceptional electrical conductivity, high stretchability, long-term functionality, the ability to withstand high stresses, and the capability of working with low cross-sectional area. While polymers and metals currently used in flexible technologies exhibit several drawbacks (for instance low electrical conductivity in polymers and low stretching capabilities in metals), shape memory alloys (SMAs),[13] could fulfill all the above requirements. Indeed, Cu-based SMAs have an extremely high electrical conductivity, 10^7 S m^{-1},[14] close to pure copper and silver (6×10^7 S m^{-1}).[15] Thanks to the superelastic behavior,[13] network-shaped devices designed with SMAs will be dramatically stretchable and their superelastic functionality could exceed 10^7 cycles,[16] withstanding stresses above 100 MPa even at small scale.[17,18] Then, SMAs could be excellent candidates to be used as electrical connectors in flexible electronic devices, provided that the last requirement could be fulfilled, this means that the above properties would be exhibited in a very low cross-sectional area, down to 1 µm^2 section or even less.

Among different families of SMAs, Ti-Ni is the most widespread SMA but shows a loss of reversibility during superelastic effect at small scale,[19] while, on the contrary, Cu-Al-Ni SMAs exhibit a good reproducible superelastic behavior at the nanoscale,[17,18] even after long-term cycling.[20,21] However, until now, Cu-Al-Ni has been the only Cu-based SMA family tested for superelasticity at nanoscale,[17,18,20–22] and in order to explore new SMA families, Cu-Al-Be becomes a very attractive family because at macroscopic scale, it exhibits a longer functional (superelastic) fatigue life than the Cu-Al-Ni family.[23]

Dr. V. Fuster, Dr. J. F. Gómez-Cortés, Prof. J. M. San Juan
Department of Condensed Matter Physics
Faculty of Science and Technology
University of the Basque Country
UPV/EHU, P.O. Box 644, 48080 Bilbao, Spain
E-mail: jose.sanjuan@ehu.es
Dr. V. Fuster
Instituto de Física Rosario
Consejo Nacional de Investigaciones Científicas y Técnicas (CONICET)-Universidad Nacional de Rosario
2000 Rosario, Argentina
Prof. M. L. Nó
Department of Applied Physics II, Faculty of Science and Technology
University of the Basque Country
UPV/EHU, P.O. Box 644, 48080 Bilbao, Spain
The ORCID identification number(s) for the author(s) of this article can be found under https://doi.org/10.1002/aelm.201900741.

DOI: 10.1002/aelm.201900741

The primary purpose of the present work is approaching the first study of the superelastic behavior in Cu-Al-Be SMA micro- and nanopillars, in order to investigate whether this family of SMAs exhibits a reproducible and completely reversible recovery of the superelastic strain, associated with the stress-induced martensitic transformation, at small scale. Additionally, the results presented throughout the paper demonstrate that small features of this SMA family exhibit a size effect on the critical stress for superelasticity and then we analyze the scaling power law that rules such phenomenon, which becomes a universal law for Cu-based SMAs. The observed behavior evidences an improvement of the superelastic performances of SMAs at small scale, which will promote their use in stretchable devices.

2. Results and Discussion

To reach the proposed goal, a Cu-12Al-0.47Be (wt%) SMA was elaborated with a concentration chosen to exhibit the orthorhombic martensitic transformation below 273 K,[24] and consequently exhibiting superelastic behavior at room temperature (see Section 4). Oriented [001] single crystals were grown from this alloy, in order to avoid any influence of the microstructure during further nanocompression tests. Polished slides cut from the single crystal were used to produce a series of micro- and nanopillars, between 2 μm and 260 nm, by focused ion beam (FIB) milling. Finally, the micro-/nanopillars were studied by nanocompression tests using an instrumented nanoindenter. All the experimental details and the procedures are carefully described in Section 4.

2.1. Superelasticity at the Nanoscale

A series of more than 20 pillars were milled and in all of them, the superelastic behavior at nanoscale was tested. In **Figure 1**a–c, the scanning electron microscopy (SEM) images, of three pillars with different diameters ϕ, are shown at different magnifications as examples of large (1520 nm), medium (780 nm), and small (295 nm) sizes. The height of the pillars, h, also varies because along the whole series an aspect ratio h/ϕ between three and five

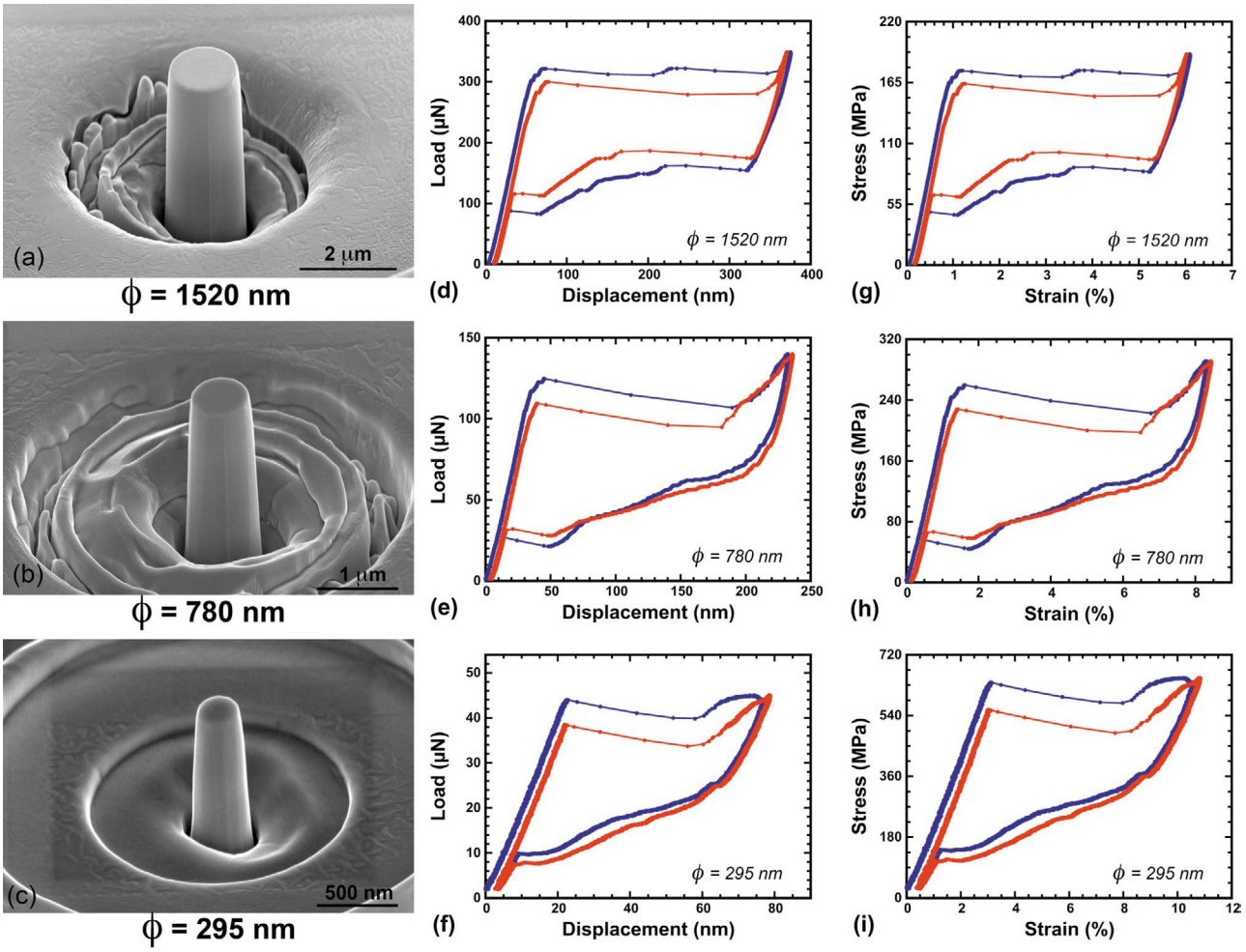

Figure 1. Scanning electron microscopy images, at different magnifications, of [001] oriented micro and nanopillars of the Cu-Al-Be SMA with different diameters ϕ: a) 1520 nm, b) 780 nm, c) 295 nm. d–f) Load–displacement curves, measured by nanocompression tests, illustrating the superelastic behavior of the pillars on the left, respectively. The first cycle (blue dots) and the second cycle (red dots) are shown in all cases. g–i) Stress–strain cycles obtained from the previous load–displacement curves, respectively.

was maintained, as recommended for microcompression tests.[25] The equipment for nanocompression tests is also able to use the diamond indenter tip as a scanning probe microscope in contact mode allowing a careful positioning of the indenter apex over the pillar. Then, multiple-cycle compression tests were carried out, along which the pillars experience essentially uniform compressive strain. The nanocompression tests were conducted under load control, to avoid any experimental artifact from feedback actions. In Figure 1d–f the first (blue) and second (red) superelastic cycles, performed on each one of the shown pillars, are plotted at the right of the corresponding images. When reaching a critical load, the stress-induced martensitic transformation occurs and a displacement of some hundred nanometers takes place under load, along a plateau progressing practically at constant force because it happens very fast in comparison with the loading rate, and later this displacement is completely recovered during unloading. Indeed, a fully closed superelastic cycle is observed, except for a residual depth of about 2–3 nm, observed after the recovery of the first cycle, see Figure 1f, which could be associated with the flattening of the top surface pillar's roughness beneath the indenter, because the second cycle becomes fully closed even at this scale. The critical load to induce the martensitic transformation undergoes a decrease during the first few cycles due to a training effect already reported in other SMAs.[20,21,26]

From the load–displacement curves, and using the measured height and diameter of each pillar, the stress–strain curves shown in Figure 1g–i are easily obtained. After the elastic strain of the austenite β phase, the critical stress is reached and the pillar transforms to martensite practically at constant stress along a fast plateau of about 5% strain. What is worthy of remark is that the critical stress increases when the size of the pillars decreases, and this evolution becomes dramatic below 800 nm in diameter. To illustrate such a strong evolution, in **Figure 2**a–c, three small pillars of diameter 520, 400, and 345 nm are shown at the same magnification SEM images, and in Figure 2d–f, their stress–strain curves for the first and second cycles are plotted at the same axes scale for comparison. In all cases, the superelastic cycles are very reproducible and fully closed, with a complete recovery of the stress-induced martensite.

2.2. Size Effect and Universal Scaling Power Law

These nanocompression tests show a dramatic increase of the critical stress when decreasing the diameter of the pillar, as can be seen in **Figure 3**a (red dots), where the critical stress measured during the first cycle, for the complete series of micro-/nanopillars, is plotted versus the diameter of the pillar. The critical stress becomes practically constant above 1000 nm pillar diameter, $\sigma_{co} = 170 \pm 5$ MPa, whereas for smaller pillars there is a dramatic increase of the critical stress for superelasticity, reaching a value of 680 MPa when the diameter of the pillar decreases down to 260 nm. Most of the pillars were tested above 100 cycles and some training is responsible for the decrease of the critical stress, taking place mainly during the first 20 cycles, after which the superelastic behavior remains stable (see Figure S1a, Supporting Information). The critical stress for the 100th cycle is also plotted versus the pillar diameter, in Figure 3a (blue dots), for comparison with the first cycle. In spite of the influence of the initial training, a clear size effect on the critical stress can be noticed even after cycling. Although the equipment is not well adapted for fatigue testing, the long-term cycling was tested in a couple of pillars, performing more than 1000 superelastic cycles. Such pillars are indicated in Figure 3a with a green circle surrounding their first cycle, and the critical stresses of the corresponding 1000th cycle are plotted as green

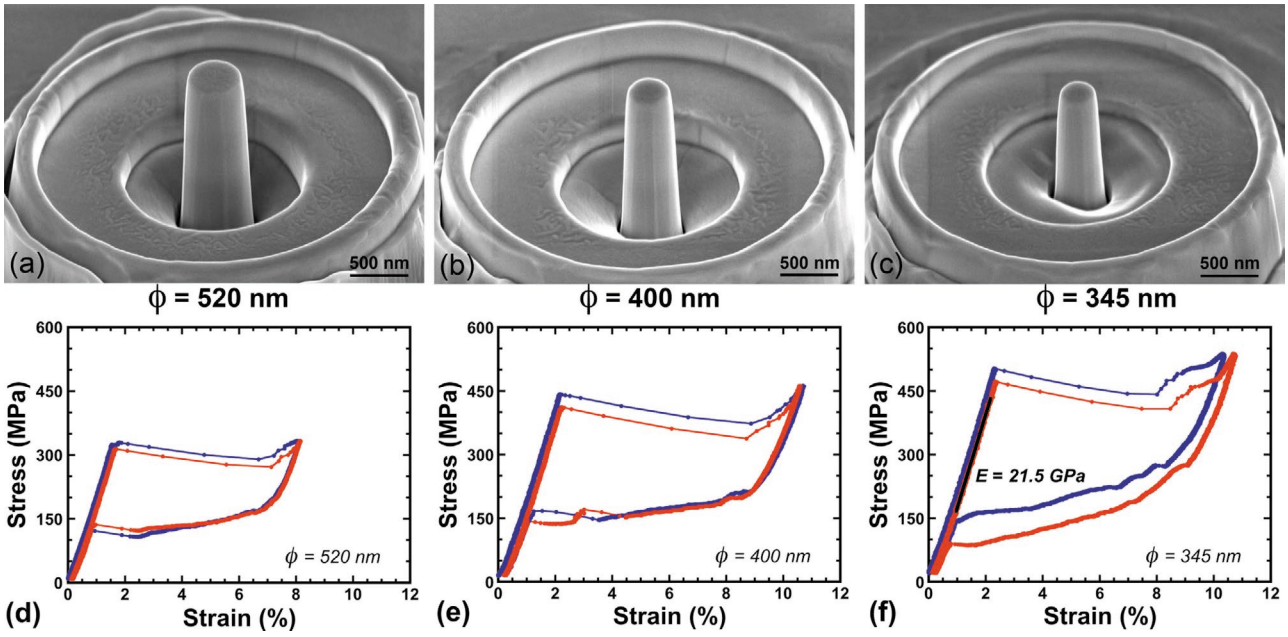

Figure 2. Scanning electron microscopy images of three [001] nanopillars of the Cu-Al-Be SMA with different diameters ϕ, at the same magnification for comparison: a) 520 nm, b) 400 nm, c) 345 nm. d–f) Stress–strain curves measured for the above nanopillars, plotted at the same scale to illustrate the dependence of the superelastic behavior on the size of the pillars. The fit of the elastic strain slope to the Young's modulus is indicated in (f).

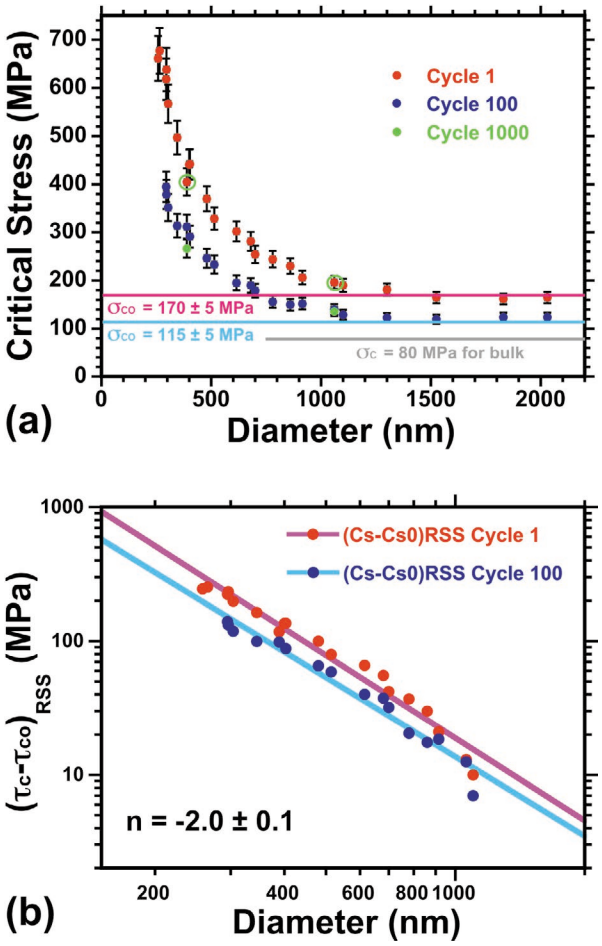

Figure 3. a) Dependence of the critical stress for superelasticity on the pillar diameter, for the complete series of micro- and nanopillars. The plot includes the critical stress measured for the first cycle (red dots), for the hundredth cycle (blue dots) and for those pillars with thousand cycles (green dots). Error bars of ±8% on the critical stress are included. The asymptotic critical stresses σ_{co} are also drawn in both cases. b) Double logarithmic plot of the resolved critical stress on the {110} planes of austenite (basal planes for martensite) versus the pillar diameter, for the results obtained during the first cycle (red dots) and the hundredth cycle (blue dots). The fitting to the straight line corresponding to Equation (2), (magenta and cyan respectively), shows that in both cases the slope of the scaling power law is $n = -2 \pm 0.1$.

dots. The evolution of the critical stress along the thousand cycles for the small pillar of 390 nm in diameter is presented in Figure S1b, Supporting Information. The comparison of the thousandth cycle with the hundredth one shows that a similar size effect will still stand for long-term cycling.

The nucleation and growth of the martensite during the stress-induced martensitic transformation at small scale can be associated with a homogeneous shearing of the atomic lattice of the austenite phase,[27] or with a heterogeneous nucleation on dislocations,[28] and we may consider in the first approach that the observed size effect could be similar to the size effect reported in confined plasticity.[29] Then, to analyze the size effect observed in Figure 3a, a scaling law similar to the one proposed for the strength of metals at small scale can be considered[30]

$$\sigma_c = \sigma_{co} + A \cdot d^n \quad (1)$$

In our case, σ_c is the critical stress for superelasticity, instead of the yield stress in confined plasticity, σ_{co} is the size-independent critical stress, which can be considered as the asymptotic value of the stress when no size effect is present, $\sigma_{co} = 170$ MPa (Figure 3a), d is the pillar diameter, A and n are empirical constants, n being the exponent of the scaling power law. As the experiments are conducted on [001] axial compression, a further refinement of Equation (1) must consider the resolved shear stress on the direction and plane of the atomic lattice shearing responsible for the stress-induced martensitic transformation; in situ transmission electron microscopy showed that at small scale this is given by the Schmid factor m_b of the {110} basal plane of martensite.[31] Using the critical resolved stress, $\tau_{cRSS} = \sigma_c \cdot m_b$, Equation (1) becomes

$$\tau_{cRSS} = \tau_{coRSS} + A' \cdot d^n \quad (2)$$

According to Equation (2), a plot of $\log(\tau_c - \tau_{co})_{RSS}$ versus $\log(d)$ allows obtaining the scaling power law exponent n as the slope of the fitted straight line. This plot is presented in Figure 3b and a value of $n = -2.0 \pm 0.1$ is fitted, with a good correlation, for both sets of experimental results, the critical stress measured during the first cycle (red dots) and the one measured after 100 cycles (blue dots). This is an outstanding result because, from a recent review on size effects,[32] the exponent n of the scaling law for confined plasticity is ranging between −0.3 and −0.8 for non-predeformed samples, being still unclear the physical meaning of this exponent. In what concerns the stress-induced martensitic transformation, a size-independent shape memory behavior was reported for Ti-Ni,[33] and no trend was revealed for superelasticity in a previous review.[32] Only in a recent work on Cu-Al-Ni SMAs,[27] an exponent of $n = -2.0$ was reported for the size effect on superelasticity. Although both families of SMAs, Cu-Al-Ni and Cu-Al-Be, have the structure of the Heusler alloys, Cu-Al-Ni has a $L2_1$ atomic order,[34] whereas Cu-Al-Be has a $D0_3$ atomic order,[24,35] and this fact could have a noticeable influence on the yield stress for plasticity as well as on the superelastic behavior. Indeed, in Cu-Al-Ni, the α' martensite, which is stress-induced in tensile experiments, is able to offer a reversible superelastic strain of 24%, but the required stress is very high, ≈500 MPa, becoming close to the fracture strength of martensite,[36] and preventing the reliable use of such transformation in practical applications. On the contrary, in Cu-Al-Be such transformation occurs at much lower stresses, ≈250 MPa,[37] and consequently is susceptible of being used to notably increase the stretching capabilities of SMAs in flexible technologies. This is an interesting advantage of Cu-Al-Be over other SMAs, which motivates the choice of this alloy family; although in this first work at nanoscale, pillars were tested in compression for technical reasons, see Section 4. However, in spite of such particularities of Cu-Al-Be SMAs, the exponent $n = -2$ found from the fitting of Figure 3b suggests to consider a similar behavior of the scaling power law associated with the size effect on superelasticity. As discussed in previous works,[18,27] the paucity of dislocations and potential nucleation points in small pillars allows to consider a scenario in which a homogeneous nucleation of the stress-induced martensite

can occur by the atomic lattice shearing of the austenite on the <011> directions over the {011} basal planes, through a critical atomic displacement U_M, when some atoms of the elastically stretched cubic austenite phase reach the atomic positions corresponding to the basal plane of the martensite lattice. Then a shuffling relaxation of the stretched bonds of the austenite lattice occurs, giving place to the nucleation of the martensite lattice. This process takes place very fast when reaching the critical crystallographic displacement U_M, and produces an abrupt jump on the stress–strain curves due to the stress-induced martensitic transformation, which is observed in all superelastic cycles, and particularly in small pillars like those of Figure 2.

The scaling law with an exponent $n = -2$ can be explained through a simple elastic model.[27] When an axial external stress σ is applied in compression on the [001] direction of a pillar, $\sigma_{zz} = -\sigma$, a compressive strain $\varepsilon_{zz} = -\sigma/E$ occurs, together with a lateral expansion associated with the radial strain $\varepsilon_{rr} = \nu\sigma/E$ and to the circumferential strain $\varepsilon_{\theta\theta} = \nu\sigma/E$, according to the rules of elasticity, which in cylindrical coordinates are remembered in the Supporting Information (E is the Young's modulus on the [001] direction and ν the Poisson ratio). The important point is that the circumferential strain $\varepsilon_{\theta\theta}$ exhibits an explicit dependence on $1/r$, which is the responsible for the exponent $n = -2$ of the scaling law. Then, the dependence of the critical stress σ_c on the pillar radius r_p, so the scaling law, will be offered by the derivative, $\partial\sigma_c/\partial r_p$, which is calculated in Equation (S6), Supporting Information. Finally, with the considerations described in the Supporting Information, the functional dependence of the critical stress for superelasticity on the pillar diameter d_p is given by

$$\sigma_c = \sigma_{co} + \frac{2\sqrt{2}\cdot E\cdot U_M}{m_b\cdot \nu}\cdot(d_o - d_p)\cdot\frac{1}{d_p^2} \quad (3)$$

Where d_o is the limit diameter above which there is no size effect. To verify whether this elastic and atomistic model works in the case of the Cu-Al-Be, we must consider values for our alloy: $E = 21.5$ GPa and $\nu = 0.472$ are calculated from the measured elastic constants,[38] $m_b = 0.5$ and $U_M = 1/6(a/\sqrt{2}) = 0.0685$ nm are calculated from the lattice parameter of the austenite $a = 0.5814$ nm.[35] In **Figure 4**, the experimental points corresponding to the critical stress measured during the first cycle (red dots) are plotted together with the data of the fitting to Equation (2), obtained from Figure 3b (blue curve), and in the same plot the fitting of the experimental points to the theoretical Equation (3), using the values for Cu-Al-Be, is also shown (green curve).

The fit to both equations is exceptionally good with an impressive coincidence between these functions, the empirical and the theoretical ones. The fit to Equation (3), letting free the unknown value of the limit diameter d_o, offers a value of $d_o = 2400$ nm, which is a quite reasonable value. For pillars with a diameter $d \geq d_o$ the local plastic deformation and heterogeneous nucleation will prevail, preventing the homogeneous nucleation mechanism. On the contrary, for pillars with diameters $d < d_o$, the size effect will be present and becomes dramatic for $d < d_o/4 \approx 600$ nm when the quadratic term firmly stands. Then, the homogeneous nucleation of martensite will be the dominant mechanism as suggested by the very abrupt superelastic strain

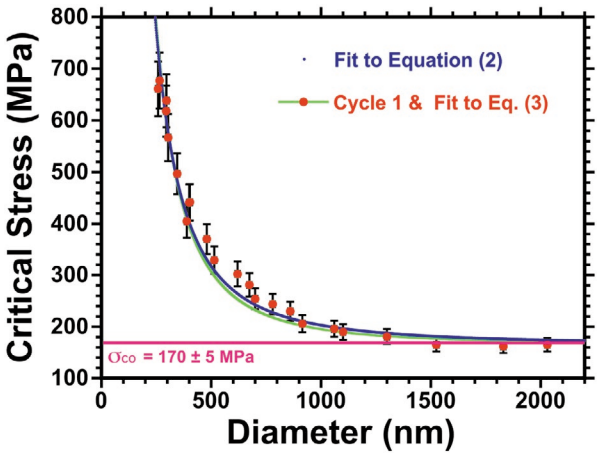

Figure 4. Experimental results of the critical stress for superelasticity versus the pillar diameter measured during the first cycle (red dots), together with the plot of the scaling power law fitted by Equation (2) in Figure 3b (blue curve), as well as with the fitting of the experimental results to Equation (3), corresponding to the model for homogeneous nucleation of martensite, using the values for Cu-Al-Be indicated in the text (green curve).

occurring when reaching the critical stress, which is clearly observed for small diameters, see Figures 1 and 2.

The found and described scaling law will hold for Cu-Al-Be, as well as for Cu-Al-Ni, provided that plastic deformation is prevented and this is favored at small scale in these SMAs because their critical stress for superelasticity is much lower than the yield point of the austenite phase. On the contrary, in Ti-Ni SMAs, the critical stress required to induce the transformation is rather high, whereas the yield point for plasticity in non-aged samples is very low, see the review by Otsuka and Ren.[39] In aged samples, the Ti_3Ni_4 precipitates produce a strong strain-hardening during the stress-induced transformation, which impedes the recovery, giving place to a non-recoverable plastic strain, even in single crystals at small scale.[19,33]

The above discussion also allows to understand why the scaling law exponent for superelasticity $n = -2$ is very different from the one found for confined plasticity in body-centered cubic (bcc) metals, between –0.3 and –0.8.[32] Although the austenite in Cu-based Heusler alloys is bcc, the mechanism behind the size effect in both cases is completely different, in superelasticity is due to a lattice shearing associated with a structural phase transformation, whereas in confined plasticity is ruled by density, nucleation, and motion of dislocations.[32]

The same methodology presented in Figure 4 was also used to analyze the data shown in Figure 3 for the hundredth cycle, and is presented in Figure S2, Supporting Information. The influence of cycling is not only a decrease of the critical stress for superelasticity, as shown in Figure 3a, but also a decrease of the limit diameter $d_o = 1600$ nm, when the same parameters for Cu-Al-Be are used to fit the experimental results to the homogeneous nucleation model given by Equation (3). Both effects can be rationalized in a scenario where the training by cycling generates some defects, stacking faults, or surface defects, requiring a smaller critical lattice shearing to promote the nucleation of martensite and consequently the nucleation and further growth of martensite occur at slightly lower critical

stress for cycled pillars. In any case, the scaling power law with exponent $n = -2$ still holds, emerging as a universal law for the Cu-based SMAs.

3. Conclusions

In summary, the presented experimental results demonstrate that Cu-Al-Be SMAs exhibit a reproducible and fully recoverable superelastic effect, above 8% strain, at micro-/nanoscale down to 260 nm in diameter. Then, the requirement of functionality for sections below 1 μm^2 is largely fulfilled, paving the way for using these alloys in flexible and wearable electronics. In addition, the observed behavior evidences that there is an important size effect on the critical stress for superelasticity and a scaling power law with exponent $n = -2$ has been found for such size effect. The model of homogeneous nucleation of the stress-induced martensite by the atomic lattice shearing of the austenite fits very well the obtained results and offers a physical understanding of such exponent. From the above results, we can conclude that the scaling power law, with $n = -2$, is verified for both Cu-Al-Ni and Cu-Al-Be SMAs and we can finally propose that it could be considered as a universal scaling law for the size effect on superelasticity in Cu-based SMAs. The final consequence of the observed size effect is that Cu-based SMAs improve their superelastic behavior at small scale, offering exceptional performances for the use as conductors in flexible electronic and wearable technologies.

4. Experimental Section

Samples and Pillar Machining: Single crystals of Cu-Al-Be SMAs were grown by the Bridgman method with an [001] oriented seed. Then, the samples were annealed at 1023 K in Ar during 1800 s and quenched in boiling water at 373 K to freeze the metastable austenitic phase at room temperature and to avoid further evolution of the transformation temperatures.[40] The chemical composition Cu-12Al-0.47Be (wt%) was chosen in order to conduct the superelastic tests at room temperature,[24] and indeed the transformation temperatures measured by differential scanning calorimetry (DSC) were $M_s = 247$ K, $M_f = 194$ K, $A_s = 233$ K, $A_f = 263$ K (martensite start and finish, and austenite start and finish, respectively). Samples ≈ 3 mm thick were cut from the single crystal and mechanically grinded and polished. Micro- and nanometer-scale pillars were milled by FIB, in a FEI Helios 650 Nanolab at the General Services SGIKER of the University of the Basque Country. The standard milling conditions were 30 kV and a series of decreasing current steps down to 24 pA with finishing steps at 15 and 7.7 pA, to minimize potential Ga damage and contamination.[18,27] All [001] oriented pillars were milled in the center of a crater, more than 50 µm apart from each other, according to the procedure previously described for similar SMAs.[17,41] SEM images were acquired with the same equipment.

Nanocompression Tests: Nanocompression experiments were performed using a Hysitron Triboindenter TI-950, equipped with a 2 µm radius sphero-conical diamond tip. The procedure followed was described in detail in previous works.[17,41] Working in scanning probe microscopy mode, the images of the pillars at a fixed contact load of 2 µN allowed a careful positioning of the tip apex on top of each pillar. A load function of multiple-cycle was used for the nanocompression tests (typically five cycles) and to avoid any experimental artifact from the electronic feedback, a constant loading–unloading rate was used, with values ranging from 150 µN s^{-1} for pillar diameters above 1 µm, down to 10 µN s^{-1} for the smallest pillar diameter of 260 nm. The Triboindenter works in an air-conditioned room and the temperature was measured during the tests with a sensor incorporated at the bridge of the TI-950; 298 ± 1 K was maintained along all the tests. Thermal drift was analyzed and automatically corrected by the TriboScan software. The procedure to convert the raw load–displacement data into stress–strain curves was previously described.[27] The cross section is determined by measuring the pillar diameter below the top circle in the 45° tilted view at the SEM, in order to avoid any wrong estimation coming from the rounding and tapering effects of FIB milling. The effective height of the pillars was obtained by a linear fit of the elastic part of the stress–strain plot, to the real value of the E [001] elastic Young's modulus in macroscopic single crystals of Cu-Al-Be with the same orientation and similar composition, E [001] = 21.5 GPa, determined from the elastic constants.[38] This procedure offers an error bar of 10 nm in the pillar diameter and 8% in the critical stress for superelasticity, which are considered in Figures 3 and 4.

Supporting Information

Supporting Information is available from the Wiley Online Library or from the author.

Acknowledgements

This work was supported by the Spanish Ministry of Economy and Competitiveness, MINECO, projects MAT2017-84069P and CONSOLIDER-INGENIO 2010 CSD2009-00013, as well as by the ELKARTEK-ACTIMAT project from the Industry Department of the Basque Government, and GIU-17/071 from the University of the Basque Country, UPV/EHU. This work made use of the FIB facilities of the SGIKER from the UPV/EHU. V.F. also acknowledges the Post-Doctoral Mobility Grant from the CONICET of Argentina, and J.F.G.-C. acknowledges the Post-Doctoral Grant (ESPDOC18/37) from the UPV/EHU.

Conflict of Interest

The authors declare no conflict of interest.

Keywords

nanocompression, shape-memory alloys, size effects, stretchable materials, superelasticity

Received: July 18, 2019
Revised: October 18, 2019
Published online:

[1] W. Zeng, L. Shu, Q. Li, S. Chen, F. Wang, X. M. Tao, *Adv. Mater.* **2014**, *26*, 5310.
[2] D. J. Lipomi, Z. Bao, *MRS Bull.* **2017**, *42*, 93.
[3] a) J. Xu, S. Wang, G-J. N. Wang, C. Zhu, S. Luo, L. Jin, X. Gu, S. Chen, V. R. Feig, J. W. F. To, S. Rondeau-Gagné, J. Park, B. C. Schroeder, C. Lu, J. Y. Oh, Y. Wang, Y-H. Kim, H. Yan, R. Sinclair, D. Zhou, G. Xue, B. Murmann, C. Linder, W. Cai, J. B-H. Tok, J. W. Chung, Z. Bao, *Science* **2017**, *355*, 59; b) K. Myny, *Nat. Electron.* **2018**, *1*, 30.
[4] S. Walia, C. M. Shah, P. Gutruf, H. Nili, D. R. Chowdhury, W. Withayachumnankul, M. Bhaskaran, S. Sriram, *App. Phys. Rev.* **2015**, *2*, 011303.

[5] S. Bauer, S. Bauer-Gogonea, I. Graz, M. Kaltenbrunner, C. Keplinger, R. Schwödiauer, *Adv. Mater.* **2014**, *26*, 149.
[6] a) L. Hines, K. Petersen, G. Z. Lum, M. Sitti, *Adv. Mater.* **2017**, *29*, 1603483; b) C. Wang, K. Sim, J. Chen, H. Kim, Z. Rao, Y. Li, W. Chen, J. Song, R. Verduzco, C. Yu, *Adv. Mater.* **2018**, *30*, 1706695.
[7] a) D.-H. Kim, N. Lu, R. Ma, Y.-S. Kim, R.-H. Kim, S. Wang, J. Wu, S. M. Won, H. Tao, A. Islam, K. J. Yu, T.-I. Kim, R. Chowdhury, M. Ying, L. Xu, M. Li, H.-J. Chung, H. Keum, M. McCormck, P. Liu, Y.-W. Zhang, F. G. Omenetto, Y. Huang, T. Coleman, J. A. Rogers, *Science* **2011**, *333*, 838; b) R. C. Webb, A. P. Bonifas, A. Behnaz, Y. Zhang, K. J. Yu, H. Cheng, M. Shi, Z. Bian, Z. Liu, Y.-S. Kim, W.-H. Yeo, J. S. Park, J. Song, Y. Li, Y. Huang, A. M. Gorbach, J. A. Rogers, *Nat. Mater.* **2013**, *12*, 938; c) X. Wang, L. Dong, H. Zhang, R. Yu, C. Pan, Z. L. Wang, *Adv. Sci.* **2015**, *2*, 1500169; d) A. Chortos, J. Liu, Z. Bao, *Nat. Mater.* **2016**, *15*, 937; e) T. Someya, S. Bauer, M. Kaltenbrunner, *MRS Bull.* **2017**, *42*, 124.
[8] S. M. Wellman, J. R. Eles, K. A. Ludwig, J. P. Seymour, N. J. Michelson, W. E. McFadden, A. L. Vazquez, T. D. Y. Kozai, *Adv. Funct. Mater.* **2018**, *28*, 1701269.
[9] S. Choi, S. I. Han, D. Jung, H. J. Hwang, C. Lim, S. Bae, O. K. Park, C. M. Tschabrunn, M. Lee, S. Y. Bae, J. W. Yu, J. H. Ryu, S.-W. Lee, K. Park, P. M. Kang, W. B. Lee, R. Nezafat, T. Hyeon, D.-H. Kim, *Nat. Nanotechnol.* **2018**, *13*, 1048.
[10] The Global Market for Printable, Flexible and Stretchable Sensors and Electronics 2017–2027, Future Markets Inc., Edinburgh, UK **2017**.
[11] S. Wagner, S. Bauer, *MRS Bull.* **2012**, *37*, 207.
[12] M. Behl, M. Y. Razzaq, A. Lendlein, *Adv. Mater.* **2010**, *22*, 3388.
[13] a) K. Otsuka, C. M. Wayman, *Shape Memory Materials*, Cambridge University Press, Cambridge **1998**; b) K. Yamauchi, I. Ohkata, K. Tsuchiya, S. Miyazaki, *Shape Memory and Superelastic Alloys*, Woodhead Publishing. Cambridge **2011**.
[14] P. Tautzenberger, in *Engineering Aspects of Shape Memory Alloys* (Eds: T. W. Duerig, K. N. Melton, D. Stockel, C. M. Wayman), Butterworth-Heinemann, London **1990**, 207.
[15] P. L. Rossiter, *The Electrical Resistivity of Metals and Alloys*, Cambridge University Press, Cambridge **1987**.
[16] a) C. Chluba, W. Ge, R. L. Miranda, J. Strobel, l. Kienle, E. Quandt, M. Wuttig, *Science* **2015**, *348*, 1004; b) H. Gu, L. Bumke, C. Chluba, E. Quandt, R. D. James, *Mater. Today* **2018**, *21*, 265.
[17] J. M. San Juan, M. L. Nó, C. A. Schuh, *Adv. Mater.* **2008**, *20*, 272.
[18] J. M. San Juan, M. L. Nó, C. A. Schuh, *Nat. Nanotechnol.* **2009**, *4*, 415.
[19] C. P. Frick, S. Orso, E. Arzt, *Acta Mater.* **2007**, *55*, 3845.
[20] J. San Juan, J. F. Gómez-Cortés, G. A. López, C. Jiao, M. L. Nó, *Appl. Phys. Lett.* **2014**, *104*, 011901.
[21] J. F. Gómez-Cortés, M. L. Nó, I. Ruíz-Larrea, T. Breczewski, A. López-Echarri, C. A. Schuh, J. M. San Juan, *Acta Mater.* **2019**, *166*, 346.
[22] L. Liu, X. Ding, J. Li, T. Lookman, J. Sun, *Nanoscale* **2014**, *6*, 2067.
[23] a) H. Sakamoto, *Trans. Jpn. Inst. Met.* **1983**, *24*, 665; b) N. Siderey, A. Hautcoeur, A. Eberhardt, *Mater. Sci. Eng., A* **2005**, *396*, 296.
[24] S. Belkahla, H. Flores-Zuñiga, G. Guenin, *Mater. Sci. Eng., A* **1993**, *169*, 119.
[25] H. Zhang, B. E. Schuster, Q. Wei, K. T. Ramesh, *Scr. Mater.* **2006**, *54*, 181.
[26] J. M. San Juan, M. L. Nó, C. A. Schuh, *Acta Mater.* **2012**, *60*, 4093.
[27] J. F. Gómez-Cortés, M. L. Nó, I. López-Ferreño, J. Hernández-Saz, S. I. Molina, A. Chuvilin, J. M. San Juan, *Nat. Nanotechnol.* **2017**, *12*, 790.
[28] A. Ibarra, D. Caillard, J. San Juan, M. L. Nó, *Appl. Phys. Lett.* **2007**, *90*, 101907.
[29] a) M. D. Uchic, D. M. Dimiduk, J. N. Florando, W. D. Nix, *Science* **2004**, *305*, 986; b) K. Gall, J. Diao, M. L. Dunn, *Nano Lett.* **2004**, *4*, 2431; c) J. R. Greer, W. C. Oliver, W. D. Nix, *Acta Mater.* **2005**, *53*, 1821.
[30] R. Dou, B. Derby, *Scripta Mater.* **2009**, *61*, 524.
[31] M. L. Nó, A. Ibarra, D. Caillard, J. San Juan, *Acta Mater.* **2010**, *58*, 6181.
[32] J. R. Greer, J. T. M. De Hosson, *Prog. Mater. Sci.* **2011**, *56*, 654.
[33] B. G. Clark, D. S. Gianola, O. Kraft, C. P. Frick, *Adv. Eng. Mater.* **2010**, *12*, 808.
[34] J. I. Pérez-Landazabal, V. Recarte, R. B. Pérez-Sáez, M. L. Nó, J. Campo, J. San Juan, *Appl. Phys. Lett.* **2002**, *81*, 1794.
[35] L. Mañosa, M. Jurado, A. González-Comas, E. Obradó, A. Planes, J. Zarestky, C. Stassis, R. Romero, A. Somoza, M. Morin, *Acta Mater.* **1998**, *46*, 1045.
[36] a) K. Otsuka, H. Sakamoto, K. Shimizu, *Acta Metall.* **1979**, *27*, 585; b) V. Novák, J. Malimánek, N. Zárubová, *Mater. Sci. Eng., A* **1995**, *191*, 193; c) P. Sittner, V. Novák, *J. Eng. Mater. Technol.* **1999**, *121*, 48.
[37] a) R. Amireche, M. Morin, in *Int. Conf. on Martensitic Transformations – 2008* (Eds: G. B. Olson, D. S. Lieberman, A. Saxena), TMS, Pittsburg, CA **2009**, 577; b) F. de Castro Bubani, M. Sade, V. Torra, F. Lovey, A. Yawny, *Mater. Sci. Eng., A* **2013**, *583*, 129.
[38] A. Planes, L. Mañosa, D. Ríos-Jara, J. Ortín, *Phys. Rev. B* **1992**, *45*, 7633.
[39] K. Otsuka, X. Ren, *Prog. Mater. Sci.* **2005**, *50*, 511.
[40] I. López-Ferreño, T. Breczewski, I. Ruíz-Larrea, A. López-Echarri, M. L. Nó, J. San Juan, *J. Alloys Compd.* **2013**, *577S*, S463.
[41] J. San Juan, M. L. Nó, C. A. Schuh, *J. Mater. Res.* **2011**, *26*, 2461.